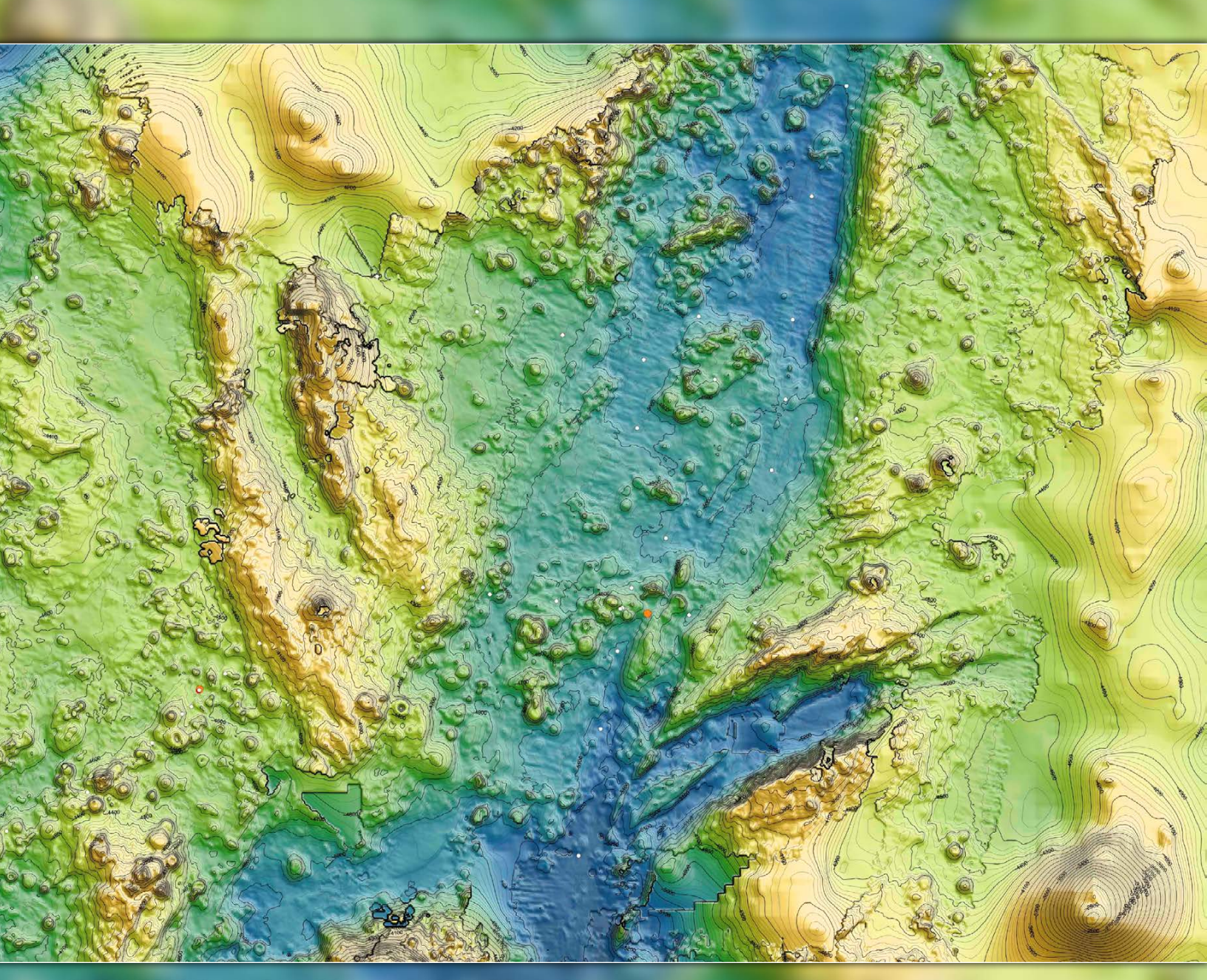
FLOW-TOPOGRAPHY INTERACTIONS IN THE SAMOAN PASSAGE

By James B. Girton, John B. Mickett, ZhongXiang Zhao, Matthew H. Alford, Gunnar Voet, Jesse M. Cusack,
Glenn S. Carter, Kelly A. Pearson-Potts, Larry J. Pratt, Shuwen Tan, and Jody M. Klymak



High-resolution bathymetry from multibeam sonar collected during the Samoan Passage 2011 mapping cruise on R/V Kilo Moana. Credit: Gunnar Voet

The response to large- and small-scale topographic features can include both lateral steering and vertical mixing.

ABSTRACT. Mixing in the Samoan Passage has implications for the abyssal water properties of the entire North Pacific—nearly 20% of the global ocean's volume. Dense bottom water formed near Antarctica encounters the passage—a gap in a ridge extending from north of Samoa eastward across the Pacific at around 10°S—and forms an energetic cascade much like a river flowing through a canyon. The 2011-2014 Samoan Passage Abyssal Mixing Experiment explored the importance of topography to the dense water flow on a wide range of scales, including (1) constraints on transport due to the overall passage shape and the heights of its multiple sills, (2) rapid changes in water properties along particular pathways at localized mixing hotspots where there is extreme topographic roughness and/or downslope flow acceleration, and (3) diversion and disturbance of flow pathways and density surfaces by small-scale seamounts and ridges. The net result is a complex but fairly steady picture of interconnected pathways with a limited number of intense mixing locations that determine the net water mass transformation. The implication of this set of circumstances is that the dominant features of Samoan Passage flow and mixing (and their responses to variations in incoming or background properties) can be described by the dynamics of a single layer of dense water flowing beneath a less-dense one, combined with mixing and transformation that is determined by the small-scale topography encountered along flow pathways.

IN PLAIN WORDS. Measurements of near-bottom currents, temperature, and salinity from high-resolution ship surveys illustrate the complexity of flow patterns around bumps, channels, and ridges in the Samoan Passage. The passage is the main source of Antarctic-origin bottom water for the North Pacific, and thus mixing rates here influence the properties and residence times of much of the deep ocean.

INTRODUCTION

Topographic blocking, steering, and stirring of near-bottom flows involves a number of dynamical regimes and balances that have been the subjects of much theoretical and numerical study, but few observational programs have been able to capture the range of scales involved. In the abyssal northward flows of Antarctic Bottom Water, the observational challenge is particularly difficult due to the large depths and broad scales involved.

Theoretical work has explored the dynamics of large-scale abyssal flow toward the equator using two-dimensional, reduced-gravity dynamics (Choboter and Swaters, 2003) and simplified one-dimensional models describing the cross-stream structure at key gaps (Whitehead et al., 1974; Gill, 1977; Killworth and MacDonald, 1993; Borenäs and Nikolopoulos, 2000). Locally, the influence of topography is often felt through acceleration and hydraulic criticality (when the flow speed

reaches the speed of the information-carrying waves), leading to diapycnal mixing through shear instability, breaking lee waves, and hydraulic jumps (Thorpe et al., 2018).

Several dynamical questions about the place of the Samoan Passage in the large-scale ocean circulation hinge on the total dense water transport and how it might change under future climate scenarios. On the largest scales, the constriction of the Samoan Passage is not an absolute constraint because the ridge ends further to the east, at the Manihiki Plateau. An important question for the Samoan Passage, then, is how much transport it can accommodate before upstream wave propagation leads to blocking and diversion around the entire ridge (Pratt et al., 2019).

Interestingly, the Samoan Passage was initially found to be one of the few abyssal water choke points in which transport agrees well with the prediction of the simplest rotating hydraulic theory that is, assuming the flow starts from a deep upstream reservoir and preserves its total angular momentum (also known as "potential vorticity," abbreviated PV) in response to latitude and layer thickness changes as it flows through the passage and over sills (Whitehead, 1998). Following up on this agreement, Freeland (2001) arrived at a lower transport prediction using more recent Samoan Passage observations, and our latest data set finds lower transport still (Voet et al., 2016).

Another question is how the transport is partitioned among the various channels and gaps that make up the Samoan Passage. Limited attempts have been made to extend the simple PV-conservation theory to multiple channels (Whitehead, 2003; Rabe et al., 2004), but a more suitable analog may be the flow of air around mountains and through gaps that has been studied with the use of laboratory and numerical models (Baines, 1995; Gaberšek and Durran, 2004).

In the end, no single simple theory can hope to span the complexity of a multi-channel flow such as that in the Samoan Passage, but it may be possible to tie multiple theoretical approaches together to arrive at an appropriate end result. Key among these is the need for a flow pathway set by the boundary conditions (upstream dense water inflow and downstream receiving basin stratification) and broad-scale topography (sill depths and channel widths and connections) before the influence of smallerscale structures (sill shape, "stirring rods," and lee wave-generating bumps) can be evaluated. In principle, this path or set of paths could be described using a coarse-resolution numerical model, but the approach taken here is to present the characteristics of the observed flow in order to suggest future directions for model simulation or parameterization. These characteristics include the overall pathways taken by the dense layer through the passage as well as the complex patterns of flows around and between small-scale obstacles. The response to large- and small-scale topographic features can include both lateral steering and vertical mixing, so the first step is to clarify which of these dominates in each of the various locations of importance. Much of the work on the 2012-2014 Samoan Passage data set to date has focused on the vertical mixing and topographic lee wave component (Alford et al., 2013; Voet et al., 2015), so it is the intention of this manuscript to highlight the lateral blocking and steering processes.

THE SAMOAN PASSAGE ABYSSAL MIXING EXPERIMENT

The Samoan Passage, a set of gaps in the east-west ridge at roughly 10°S in the Pacific north of the Samoan Islands, is a principal conduit for the northward flow of Antarctic-origin bottom water in the deep western boundary current (DWBC) from the South Pacific (Reid and Lonsdale, 1974; Johnson et al., 1994; Roemmich et al., 1996; Rudnick, 1997).

As a means to both identify long-term changes occurring in the abyssal circulation and explore topographic influences on mixing and bottom water properties, a field program was undertaken from 2011 to 2014 in the Samoan Passage. The experimental goals were to (1) constrain the overall volume budget and circulation through the multiple channels; (2) identify the dynamical processes controlling the transport and pathway selection; (3) identify the processes and locations dominating turbulence, mixing, and transformation, and (4) quantify mixing rates and parameter dependencies to aid in the representation of the Samoan Passage and similar types of mixing in circulation models.

During three cruises—a multibeam mapping survey in 2011, a large-scale hydrographic survey ("Pathways" cruise) in 2012 (Alford et al., 2013; Voet et al., 2015), and a set of high-resolution surveys of three particular focus areas ("Process" cruise) in 2014—the topographic structure, flow pathways, water mass structure, and mixing geography (Carter et al., 2019, in this issue) were characterized and studied in greater detail than ever before. Tools included ship-based surveys and mooring deployments (from two days to 17 months in length) to clarify the principal modes of spatial and temporal variability in the dense layer flow.

METHODS

Ship-based measurements were collected with a conductivity-temperature-depth (CTD) measurement package with upand down-looking acoustic Doppler current profilers ("lowered" ADCP, or LADCP, measuring horizontal currents at roughly 10 m resolution) for both single profiles and continuous tow-yos (vertical cycling of the package while the ship moves slowly along a survey track). In addition, numerous profiles of turbulent kinetic energy dissipation and diffusivity were made using a full-depth freefalling Rockland Vertical Microstructure Profiler (VMP) equipped with temperature and shear sensors. Sampling included large-scale transects designed to map the entire passage (a 100 × 200 km region) and focused high-resolution surveys around particular sills and mixing hotspots (primarily using tow-yos). In addition, short-term (2-27 day) and long-term (17 month) moored time series data were collected at a number of locations to measure temperature, salinity, and currents every 1.5 hours using vertically profiling wire crawlers or more often using fixed-depth instruments. These mooring data allow us to quantify the magnitude of tidal and other fluctuations and to clarify the degree to which apparent spatial structures in the tow-yos could be the result of temporal variability. Voet et al. (2016) report on the longest temporal scales in the moorings, and higher frequency processes are described by Cusack et al. (2019) and Pearson-Potts (2019). This paper focuses on the spatial structure seen in the ship surveys and also includes mooring averages and tidal amplitudes for comparison.

Large-Scale Survey

The Pathways survey occupied stations over the entire Samoan Passage region (Figure 1). Most of these included simultaneous CTD/LADCP and VMP profiles, undertaken by deploying the slow-falling VMP before the CTD and recovering it afterward. This allowed near-simultaneous collection of temperature, salinity, velocity, and microstructure profiles. The principal results from the large-scale survey, including passage transports and layer budgets, are detailed in Voet et al. (2015).

Hotspot Surveys

On the 2014 Process cruise, the focus turned to specific sites where the greatest flow acceleration and mixing were observed in the 2012 survey. Two of these were the sequential choke points along the eastern channel, and the third was a sill on the western path (Figure 1). The sequential sills (P4 and P5) were chosen in order to investigate the possibility of distinct varieties of hydraulic control at each, while the western path sill (P2) had been seen in the initial survey to contain dramatically different mixing patterns on two approximate streamlines only a short distance away from each other (Alford et al., 2013).

The detailed surveys were conducted using tow-yos as the most effective way to gain high-resolution information. These involved the ship moving at 0.5–0.7 knots while cycling the CTD/LADCP package between 3,600 m depth and 40 m above the bottom. Although the measurements are a snapshot of a time-varying field (with tidal aliasing sometimes presenting significant challenges to interpretation), we also employed a powerful aid in estimating and separating spatial and temporal variations by installing short-term (2-27 day) moorings in each region. The repeated mooring profiles allowed statistical and tidal characterization of not only the currents and hydrographic properties but also turbulent processes (dissipation rates), using density overturns (Cusack et al., 2019).

Single-Layer Definition

This paper describes the spatial structure of the bulk dense-layer flow through the Samoan Passage. Previous work (Reid and Lonsdale, 1974; Voet et al., 2015) considered the flow of water colder than 1°C, an isotherm found near the middle of a maximum in stratification throughout our domain. However, both stratification and shear persist within the layer. In fact, Voet et al. (2015) showed that the layer colder than 0.7°C has a distinctly different behavior, with most of this coldest water flowing through the east-

ern channel. Nevertheless, the 1°C isotherm is probably the simplest and most appropriate boundary for considering the layer of Antarctic-origin water as a whole. Throughout this paper (apart from Figure 1, which includes both 1°C and 0.7°C layer transports), flow vectors indicate the vertically integrated transport below 1°C, and all discussion will refer to the dense layer defined in this way.

RESULTS AND DISCUSSION

Figure 1 shows the overall pattern of dense layer flow through the Samoan

Passage. Transport is split between the two major pathways, steers around topographic obstacles, and accelerates over sills and through constrictions. Spatial variations in the integrated layer transport tend to be less than those in either layer thickness (h = 200-1,500 m) or velocity (u = 0.05-0.4 m s⁻¹), with typical transports around 100 m² s⁻¹ corresponding to, for example, (a) 0.1 m s⁻¹ flow in a 1,000 m layer, (b) 0.2 m s⁻¹ flow in a 250 m layer (see Figure 2 for typical layer thickness variations in space).

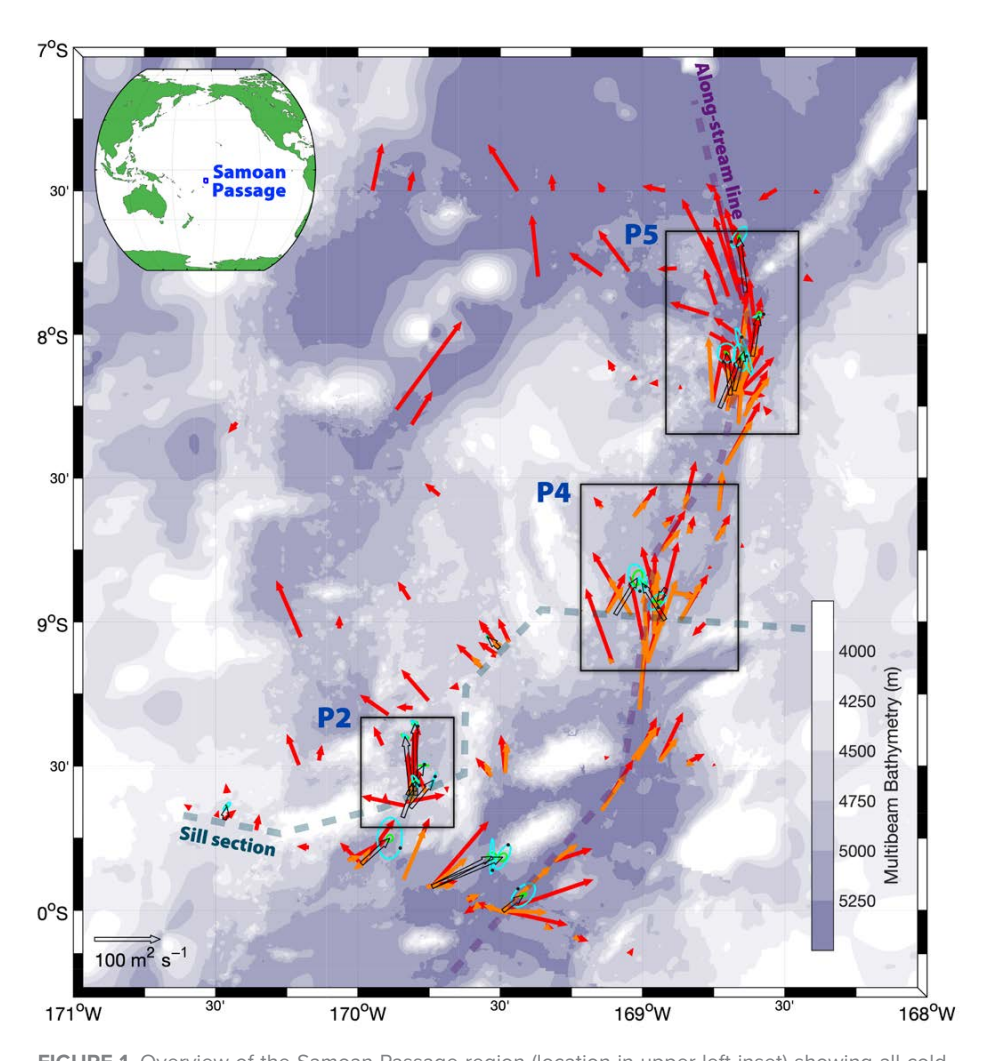


FIGURE 1. Overview of the Samoan Passage region (location in upper-left inset) showing all cold-layer transport measurements from single-station lowered acoustic Doppler current profiler (LADCP) data taken during the 2012 Pathways cruise (red arrows for <1°C and orange for <0.7°C transport). The figure also shows mooring average transports (durations from two days to 17 months) from both 2012 and 2014 cruises (open black arrows for <1°C, plus scale arrow at lower left). Mooring arrows also include diurnal (K1 in green) and semidiurnal (M2 in light blue) tidal ellipses centered on each arrowhead, with phase indicated by a small black dot. Focused hotspot survey regions at sills designated P2, P4, and P5 are framed, and high-resolution tow-yo transports from these regions are shown in Figures 4–7. Two particular sections (the "along-stream line" in purple and the cross-channel "sill section" in blue-green) are indicated with dashed lines and plotted in detail in Figures 2 and 3.

Rotating Hydraulic Transport

Hydrographic section properties and isopycnal layer volume transports are described by Voet et al. (2015), who show approximately equal total transport in the east and west passages but nearly all of the water colder than 0.7°C taking the eastern channel. This separation appears to be due to a combination of factors: (1) the sill height is deeper in the east, (2) the overall interface tilt across the passage (setting up the geostrophic pressure gradient) allows a similar amount of water in the west despite higher sills, and (3) bottom Ekman layer dynamics (the net result of frictional and Coriolis forces) tends to push the densest (i.e., coldest) water to the east. Figure 3 shows a composite section across the main controlling sills of the Samoan Passage that illustrates the obstacle presented to the large-scale flow by the ridge. The DWBC approaches from the south and preferentially flows through the westernmost pathway (left-hand passages) unless it is unable to accommodate the full transport, in which case channels to the right are progressively added. In the case of deeper isopycnals bounding a denser sub-layer, only the easternmost passage is available.

In its basic structure, the Samoan Passage dense flow is similar to that through a number of other deep ocean choke points, suggesting the likely applicability of single-layer rotating hydraulic theories for describing the transport (Q) and dynamics (Whitehead et al., 1974; Gill, 1977). The dominant controlling parameters for "wide" passages (wider than the Rossby deformation radius of $\sqrt{g'h}/f \approx 20$ km, and therefore strongly influenced by Earth's rotation) are $\Delta \rho / \rho$ the fractional density difference between the layer and the overlying background, and h_0 , the upstream interface height above the sill. The simplest transport formula is $Q = g'h_0^2/2f$ (where $g' = (9.8 \text{ m s}^{-2}) \Delta \rho / \rho$ is the "reduced" gravity," and $f = 2.3 \times 10^{-5} \text{ s}^{-1}$ is the Coriolis parameter), which is applicable for separated, hydraulically critical zero-PV flow through a flat-bottomed channel (Whitehead et al., 1974) but is also the maximal transport possible for single-layer geostrophic flow through an arbitrary topographic cross section (Killworth and MacDonald, 1993).

Whitehead (1998) pointed out that the hydraulic formula predicted the Samoan Passage transport better than that of many other abyssal choke points, giving Q = 7.0 Sv, which compares well with the measured 6.0 Sv transport average from an 18-month mooring array in 1992–1994 (Rudnick, 1997). However, it is worth mentioning that there is considerable potential for subjectivity in esti-

height of the 1°C isotherm above the P4 and P5 sills in Figure 2) would reduce the transport by a similar factor. The approximate cancellation of these two values is partly fortuitous, as other reasonable choices could be made from examination of the density profiles, but the compensating effects of the height and density parameters are also features of the typical large-scale flow and density structures set up across sills of this kind. As another example, Freeland (2001) applied the Whitehead (1998) formula to a later set of hydrographic measurements, estimating $\Delta \rho / \rho = 5 \times 10^{-5}$ and $h_0 = 730$ m to arrive at a transport of 5.7 Sv (which, along with the lower densities found in the abyssal layers, is a reduction consistent with the analysis of Voet et al., 2016). Although our own measurements did not extend as far away from the Samoan Passage sills as the profiles considered in these estimates, our best estimate of $\Delta \rho / \rho = 4 \times 10^{-5}$ and $h_0 = 800$ m using the Whitehead (1998) technique yields a similar transport of Q = 5.5 Sv. Additionally, the reduction in abyssal water density persisted throughout our measurement period, with a further 0.02 kg m⁻³ reduction from 1994 to 2012 on top of the 0.04 kg m⁻³ decrease from the 1974

GEOSECS data to 1994 (and even more

change at the bifurcation depth) noted

by Freeland (2001).

mating the parameters for a complex sill

flow. Whitehead (1998) used a procedure

based on density profiles far upstream

and downstream, together with the topo-

graphic sill depth, to get $\Delta \rho / \rho = 3 \times 10^{-5}$

and $h_0 = 1,050$ m, while examination of

the density change near the sill in a ver-

tical profile across the stratified inter-

face between the dense layer and the

"background" would likely arrive at sub-

stantially larger $\Delta \rho / \rho$ and smaller h_0 .

For comparison, using a typical $\Delta \rho / \rho$ of

 9×10^{-5} (the approximate density change

between the 0.7°C and 1.1°C isotherms)

would triple the transport prediction,

while the quadratic dependence of trans-

port on upstream height means that a

local estimate of $h_0 = 600$ m (roughly the

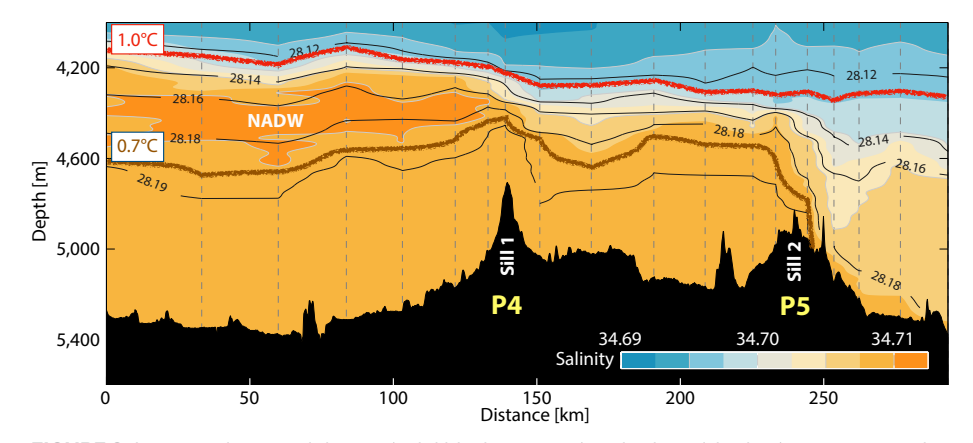


FIGURE 2. Large-scale neutral density (solid black contours) and salinity (shading) structures on the "along-stream line" in Figure 1 reveal blocking and hydraulic influence of both sills in the eastern channel (P4 and P5), plus strong mixing downstream of each. At the same time, an overall single-layer structure of anomalous dense water flowing under a quiescent, less dense layer is evident. The interfaces defined by the 1.0°C and 0.7°C isotherms are highlighted with thick lines for comparison with the full vertical structure.

Refinements to the hydraulic theory have considered how to best take the actual topographic structure of the sill cross section into account when computing transports. Borenäs and Nikolopoulos (2000) suggested a procedure that finds the maximal transport through a section by adding a variable-width stationary region while preserving the PV in the moving flow, and Whitehead (2003) additionally suggested a way to connect multiple passages using the singlevalued relationship between streamfunction and Bernoulli function (an expression of the conservation of energy in a fluid) in the flat-bottom constant-PV model. Bernoulli function and PV cannot both be constant across the section, but a varying upstream Bernoulli height (the interface obtained by converting kinetic energy back to potential) can be computed from the interface height and slope (which determines the geostrophic layer velocity). This model therefore implicitly assumes that PV conservation applies over longer distances and/or timescales than energy conservation. The magenta line in Figure 3 shows the result of an interface calculation extending across the multiple passages in the ridge crosssection using $\Delta \rho/\rho = 3 \times 10^{-5}$, an upstream interface depth of 4,040 m (setting the starting point at the left-hand side of Figure 3), and an upstream layer thickness of 860 m (setting the PV). These parameters were chosen to give an interface that reasonably approximates the top of the cold layer (as represented in different channels by different isotherms in the 0.7°-1.0°C range). The Bernoulli height (upper thin blue line in Figure 3) is used as the starting interface height (with zero initial velocity) on the next channel to the right after the interface intersects the topography (Whitehead, 2003). The total transport calculated from the computed interface (and accompanying layer thickness and geostrophic velocity) in all channels across the section in Figure 3 is 4.3 Sv. However, choosing a larger value for $\Delta \rho / \rho$ would be defensible and would result in larger transport. To more closely match the critical condition for hydraulic control, the maximization step of Borenäs and Nikolopoulos (2000) could be applied to each channel in succession—adding a flat, nonmoving, interface segment at the left side of each channel in order to position stronger velocity over the deepest part of the channel. This has not been done in Figure 3, but it is very likely that this would also increase the total transport result.

Given the range of choices implicit in using a simplified single-layer theory to predict transport of a complex sill flow, the most promising application is likely to be in using a consistent interpretation of the density structure to connect long-term changes in forcing to transport changes. For example, the new 2012-2014 transport average of 5.4 Sv (Voet et al., 2016) represents a 10% decrease from 20 years earlier, which could result from a comparable decrease in layer density anomaly, a 5% decrease in upstream height, or a combination of density and height changes. From the ~0.02°C temperature change and 50-100 m isotherm height changes presented in Voet et al. (2016), the interface height appears to be the major contributor to the transport change.

Blocking, Steering, and Mixing

Once the large-scale flow structure has selected a pathway, the along-stream evolution becomes two dimensional through stratified turbulence, with some additional three-dimensional effects evident in the small-scale lateral response to bumps and constrictions. Figures 4–7 show a selection of observed phenomena through the use of tow-yo CTD and LADCP measurements. Notable features include the following.

Lateral funneling through gaps: Flow convergence and acceleration are apparent when the flow approaches sufficiently deep gaps in sufficiently high ridges. The magnified view in Figure 7b shows the most prominent examples of this funneling through two gaps in the ridge that make up the P5 sill. In fact, the two jets created by these gaps pass to a large extent around the two short-term moorings deployed just downstream. The northernmost of these moorings displays the largest tidal variability of all locations in the Samoan Passage, in large part because it lies on the edge of the strong jet created by the funneled flow-allowing relatively small displacements of the jet to generate large fluctuations in transport (Cusack et al., 2019).

Wakes with reduced velocity behind obstacles: Not only do tall ridges block the flow, but obstacles significantly smaller than the layer thickness also have the potential to block the flow. Although there is some evidence of this in Figure 5 from the slower flows at the center of the southern P4 section, the

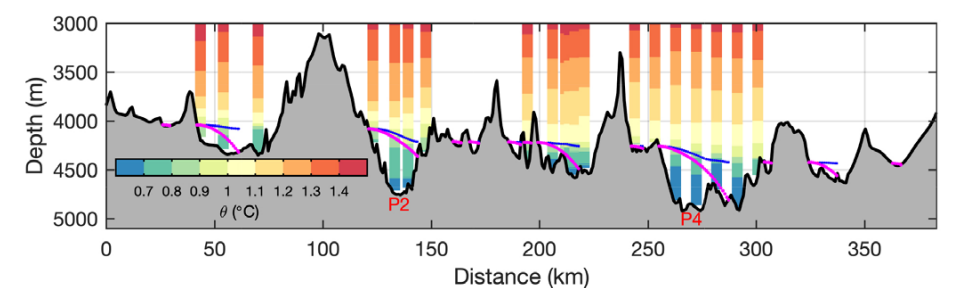


FIGURE 3. Large-scale cross-stream structure with bathymetry and temperature profiles (along the "sill section" of Figure 1) shows sloping potential temperature (θ) surfaces, consistent with geostrophically balanced northward flow. In addition, flow enhancement on the right-hand side (not shown here but evident in Figure 1 vectors and in figures in Voet et al., 2015) is consistent with potential vorticity (PV) conservation. The layer interface predicted by single-layer constant-PV rotating hydraulic theory following Whitehead (2003) is shown as a thick magenta line, and the corresponding Bernoulli height (used to predict the interface starting point in subsequent channels) is shown with a thinner blue line that lies above the magenta line.

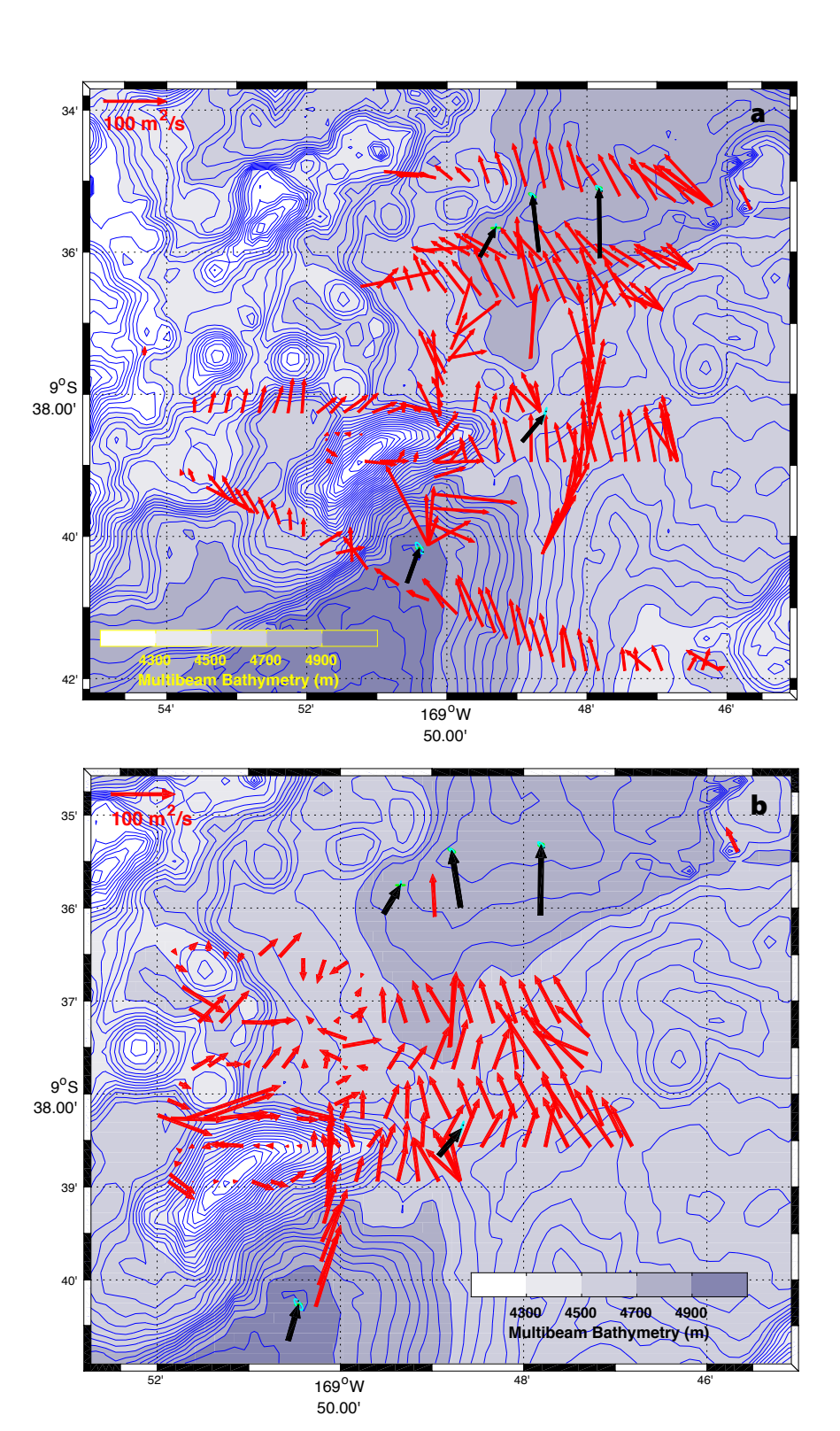


FIGURE 4. (a) Red vectors show transport of the cold (θ <1°C) layer measured with LADCP tow-yos during the Process cruise (2014) near the P2 sill (Figure 1), along with the two along-stream tow-yos from the Pathways cruise (2012) with contrasting mixing structure highlighted by Alford et al. (2013). Mean transports from profiling moorings are shown with black arrows (using the same transport scale, with M2 and K1 tidal ellipses in light blue and green, respectively). (b) Transports from additional Process cruise tow-yos near P2 (red arrows), reinforcing the disorganized flow patterns behind (north of) the topographic bump on the left-hand (west) side of the sill. Black arrows show the same mooring mean transports as in panel a. Bathymetry in 25 m intervals is contoured with thin blue lines in both panels.

best evidence is in the tow-yos around P5 shown in Figure 7a. Nearly all of the transport dips in the various sections can be connected to upstream or downstream effects of topographic features—mostly small (2–4 km wide and 100–400 m high) bumps scattered around the Samoan Passage. Another clear example just east of the northernmost mooring in Figure 7b produces a 1 km gap in the flow immediately to the north.

Overall dominance of steady flow patterns around and over topography: Most of the qualitative flow patterns persist through multiple adjacent sections and repeated occupations (even in different years), supporting the basic paradigm of a complex but steady flow responding to topography. Transport patterns measured at P2 during multiple tow-yos from the 2014 cruise (Figure 4a,b) and two from 2012 (northsouth lines in Figure 4a) illustrate the contrast between the disorganized flow north of the ridge on the west side of the sill and the fairly uniform flow over the smooth topography east of the ridge. Flow patterns at P4 (Figure 5) are surprising in both direction (northwestward flow in a northeast-trending channel) and continuity (southward flow reversal on the northern tow-yo line), but the strong agreement between the tow-yo and mooring average vectors makes it clear that these patterns are predominantly spatial rather than aliased temporal variability. Figures 6 and 7a also contain tow-yo sections repeated in both 2012 and 2014, with very little change between the two. In fact, although there is some profile-to-profile noise (jitter) in the tow-yo transports, crossover points between sections nearly always match transport direction and magnitude quite closely.

Spatially variable tidal modulation: In some locations, tidal modulation is significant, as shown by the ellipses at the ends of the mooring transport arrows in Figures 1, 4, and 5. However, tidal variability is generally a small fraction of the mean transport except on the southern line at the Samoan Passage entrance, where the slow thick cold layer allows small tidal velocities to have a large effect on trans-

port (see Figure 1). One notable exception is the T3 mooring at P5 (third cyan ellipse from the south in Figure 7) which appears to have large tidal fluctuations due to its positioning on the sharp edge of a topographic jet that is moved back and forth by the tides (see the "Lateral funneling" description above and analysis in Cusack et al., 2019).

Dynamical Regimes

It is worth considering the various flavors of dynamics that are at play in generating the complex structures seen in the transport vectors in Figures 4-7. The small- to medium-scale patterns suggest an analogy to atmospheric flows over mountains and through valleys ("gap winds") that are typically categorized in the nonrotating limit by the parameter Nh_t/u (also described as a "nondimensional height") in which N is the buoyancy frequency, h_t the topographic height, and u the flow speed (Baines, 1995; Gaberšek and Durran, 2004). At low values of Nh_t/u (<0.1; applicable to small bumps in the weakly stratified $N \sim 3 \times 10^{-4} \, \mathrm{s}^{-1}$ dense layer much less than the layer height), interface displacement and flow diversion is small and wave radiation is significant but mostly linear. At intermediate values (0.5-2, evident in the lower layer when the topographic height is comparable to the layer thickness or when interfacial flow accelerates over sills), flow may divert around obstacles but also can proceed over them-strongly influenced by topographic shape—becoming asymmetric across sills, and generating hydraulic jumps and nonlinear waves. At higher values (>10, applicable to the high ridges bounding the flow and reaching into the $N \sim 1.5 \times 10^{-3} \text{ s}^{-1}$ interface), blocking and channeling occur.

The effects of rotation are clearly evident in the large-scale cross-stream interface tilt (Figure 3) that is due to the geostrophic balance between cross-stream pressure gradient and Coriolis force. Additionally, the rotational influence of topography can appear through Taylor columns—vertical rigidity of a rotating fluid that extends to a height scale of $H \sim Lf/N$, where f/N is ~0.1 within the weakly stratified dense layer, and L is the horizontal length scale of the topographic feature (e.g., a Taylor column would be expected to extend 500 m above a 5 km wide bump). The diverted (around bumps) and channeled (through gaps) flows in Figure 7b have thicknesses of order 500 m (see Figure 2) but are influenced by features somewhat smaller in lateral extent than 5 km. They are therefore not solidly in the Taylor column regime but are affected by both rotation and the intermediate value of the blocking height parameter described above.

Similarly, rotational influence dominates when the Rossby number u/fL is small. For example, 0.1 m s⁻¹ flow over 100 km scales at the Samoan Passage entrance yields a Rossby number of 0.04 and solid justification for using rotating hydraulic theory. But the accelerated sill flows of 0.4 m s⁻¹ around small 2 km obstacles are verging on the nonrotational regime with

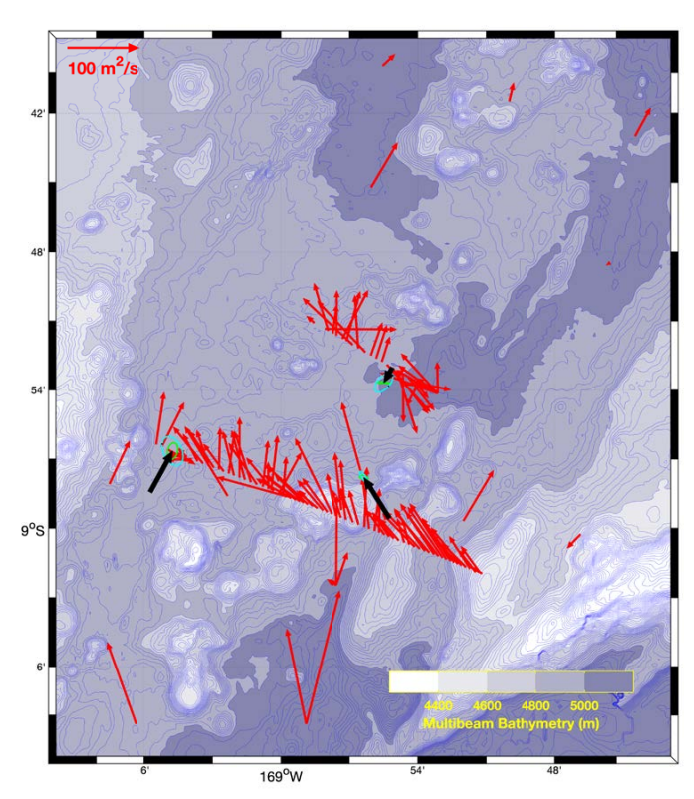


FIGURE 5. Cold ($\theta < 1^{\circ}$ C) layer transport patterns from tow-yos during the 2014 Process cruise in the P4 sill region (Figure 1) are dominated by complex but relatively steady patterns in the spatial flow structure around a series of topographic bumps. Mooring mean transports are shown with black arrows and tidal ellipses in red (M2) and green (K1). 50 m interval bathymetry contours are shown in blue.

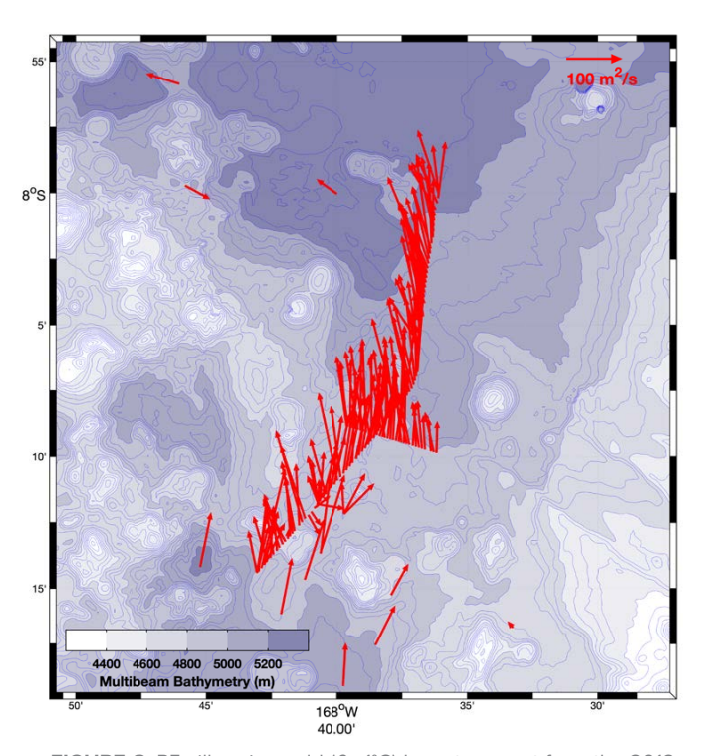


FIGURE 6. P5 sill region cold (θ <1°C) layer transport from the 2012 Survey cruise tow-yos (along-stream line shown in Figure 3 of Alford et al., 2013). Although an along-stream interpretation of this line is mostly correct, the significant cross-stream angle of the survey line suggests a role for adjacent topography in generating some of the structure. Blue denotes the 50 m interval bathymetry contours.

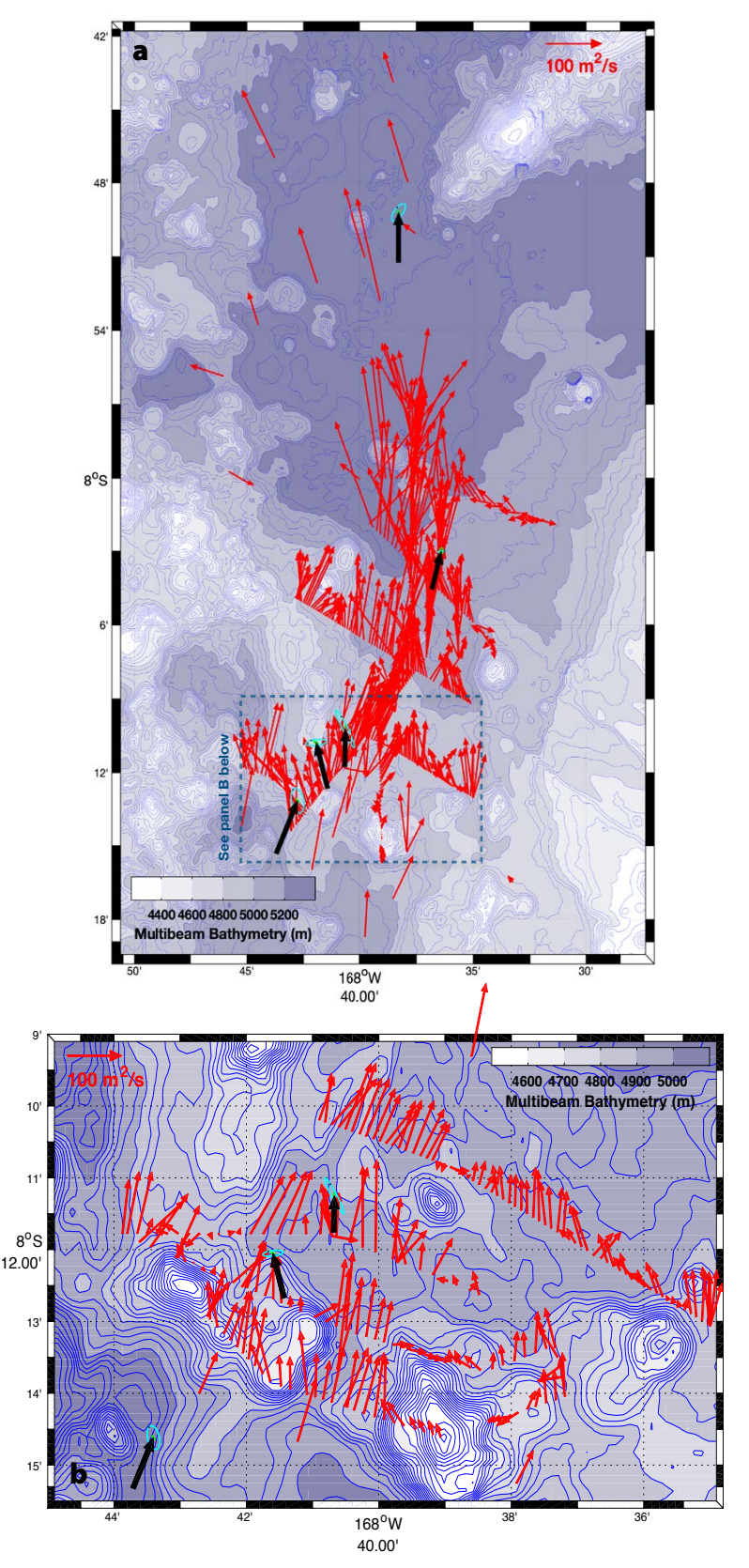


FIGURE 7. (a) P5 region θ <1°C layer transport from multiple tow-yos and moorings during the 2014 Process cruise. Blue denotes the 50 m interval bathymetry contours. (b) Additional tow-yos from the same cruise give a magnified view (location in dashed box of panel a) of the flow around bumps and through gaps in the topographic structure near the sill. Several-day mooring averages (black arrows) match well with the tow-yo snapshot vectors, again indicating a dominantly steady flow direction and magnitude. Blue denotes the 25 m interval bathymetry contours.

a Rossby number of around 10. This would argue that structures seen in the Figure 7b transport vectors are likely more dynamically related to atmospheric gap winds than to Taylor columns, while the large-scale approach of the DWBC to the Samoan Passage and the partitioning among channels seen in Figures 1 and 3 are strongly rotation-influenced processes.

CONCLUSIONS

Taken together, the flow patterns in the Samoan Passage illustrate the difficulty of developing a numerical model or mixing parameterization that can predict the net influence of the passage on the larger-scale distributions of temperature, salinity, and other tracers. Key conclusions from the maps of observed dense layer transport shown here (in Figures 1 and 4–7) include the following:

- Cross-stream structure and pathway selection (Figures 1 and 3) is reasonably well predicted by rotating hydraulic theory that assumes geostrophic currents and constant potential vorticity.
- The flow pathways also contain vertical shear in the lateral currents, with less dense layers spilling westward over the first sills encountered and the denser layers following the deepest channel to the east (Figure 1).
- On small scales, the flow develops threedimensionality due to blocking and channeling by topographic features with heights at least a significant fraction of the thickness of the dense layer (Figures 4–7).
- Time dependence is generally weak compared to the mean flow, but in some locations tidal and low-frequency variations are present (Figures 1, 5, and 7). Over the region as a whole, transport fluctuations of 20%-30% on 5-50-day timescales are common (Voet et al., 2016), but the essential patterns and pathways taken by the flow are fairly steady.
- Mixing and flow disruption by topography occurs preferentially in the choke points (e.g., sill regions P2, P4, and P5 in Figure 1) created by narrowing channels and the shallowest sills. In these locations, the flow can be well described by a nearly two-dimensional picture of shear instability, lee waves, and hydraulic jumps.

Resolving the wide range of scales that matter in Samoan Passage dynamics is a formidable task, but the salient features of the flow provide some hope—namely, that it is relatively steady and that along-path evolution is dominated by vertical (i.e., two-dimensional) mixing near major obstacles. So, there is an opportunity to simplify the dynamics by separating the path determination from the vertical mixing processes—for example, through sequential two-dimensional approaches that first predict horizontal flow pathways using single-layer dynamics or rotating hydraulic theory and later determine vertical mixing rates using the small-scale topography found along each pathway.

REFERENCES

- Alford, M.H., J.B. Girton, G. Voet, G.S. Carter, J.B. Mickett, and J.M. Klymak. 2013. Turbulent mixing and hydraulic control of abyssal water in the Samoan Passage. *Geophysical Research Letters* 40:4,668–4,674, https://doi.org/10.1002/ grl.50684.
- Baines, P.G. 1995. *Topographic Effects in Stratified Flows*. Cambridge University Press.
- Borenäs, K., and A. Nikolopoulos. 2000. Theoretical calculations based on real topography of the maximum deep-water flow through the Jungfern Passage. *Journal of Marine Research* 58:709–719, https://doi.org/10.1357/002224000321358864.
- Carter, G.S., G. Voet, M.H. Alford, J.B. Girton, J.B. Mickett, J.M. Klymak, L.J. Pratt, K.A. Pearson-Potts, J.M. Cusack, and S. Tan. 2019. A spatial geography of abyssal turbulent mixing in the Samoan Passage. *Oceanography* 32(4):194–203, https://doi.org/10.5670/oceanog.2019.425.
- Choboter, P.F., and G.E. Swaters. 2003. Twolayer models of abyssal equator-crossing flow. *Journal of Physical Oceanography* 33:1,401–1,415, https://doi.org/10.1175/1520-0485(2003)033 <1401:TMOAEF>2.0.CO;2.
- Cusack, J.M., G. Voet, M.H. Alford, J.B. Girton, G.S. Carter, L.J. Pratt, K. Pearson-Potts, and S. Tan. 2019. Persistent turbulence in the Samoan Passage. *Journal of Physical Oceanography*, https://doi.org/10.1175/JPO-D-19-0116.1.
- Freeland, H. 2001. Observations of the flow of abyssal water through the Samoa Passage. *Journal* of *Physical Oceanography* 31:2,273–2,279, https://doi.org/10.1175/1520-0485(2001)031 <2273:00TFOA>2.0.CO;2.
- Gaberšek, S., and D.R. Durran. 2004. Gap flows through idealized topography: Part I. Forcing by large-scale winds in the nonrotating limit. *Journal of the Atmospheric Sciences* 61:2,846–2,862, https://doi.org/10.1175/JAS-3340.1.
- Gill, A.E. 1977. The hydraulics of rotating-channel flow. *Journal of Fluid Mechanics* 80:641–671, https://doi.org/10.1017/S0022112077002407.
- Johnson, G., D. Rudnick, and B. Taft. 1994. Bottom water variability in the Samoa Passage. *Journal* of Marine Research 52:177–196, https://doi.org/ 10.1357/0022240943077118.
- Killworth, P.D., and N.R. MacDonald. 1993. Maximal reduced-gravity flux in rotating hydraulics. *Geophysical & Astrophysical Fluid Dynamics* 70:31–40, https://doi.org/10.1080/ 03091929308203585.
- Pearson-Potts, K.A. 2019. Deep Near-Inertial Waves in the Samoan Passage. Dissertation, University Hawai'i, Honolulu, HI, 140 pp.
- Pratt, L.J., G. Voet, A. Pacini, S. Tan, M.H. Alford, G.S. Carter, J.B. Girton, and D. Menemenlis. 2019. Pacific abyssal transport and mixing: Through the Samoan Passage versus around the Manihiki Plateau. *Journal of Physical Oceanography* 49:1,577–1,592, https://doi.org/10.1175/JPO-D-18-0124.1.

- Rabe, B., D.A. Smeed, G.F. Lane-Serff, and S.B. Dalziel. 2004. Rotating exchange flows through straits with multiple channels. Chapter 12 in International Conference: Towards a Balanced Methodology in European Hydraulic Research. Proceedings from Budapest, May 22–23, 2003.
- Reid, J., and P. Lonsdale. 1974. On the flow of water through the Samoan Passage. *Journal of Physical Oceanography* 4:58–73, https://doi.org/10.1175/1520-0485(1974)004 <0058:OTFOWT>2.0.CO;2.
- Roemmich, D., S. Hautala, and D. Rudnick. 1996. Northward abyssal transport through the Samoan Passage and adjacent regions. *Journal* of *Geophysical Research* 101:14,039–14,055, https://doi.org/10.1029/96JC00797.
- Rudnick, D. 1997. Direct velocity measurements in the Samoan Passage. *Journal of Geophysical Research* 102:3,293–3,302, https://doi.org/10.1029/ 96.JC03286.
- Thorpe, S.A., J. Malarkey, G. Voet, M.H. Alford, J.B. Girton, and G.S. Carter. 2018. Application of a model of internal hydraulic jumps. *Journal of Fluid Mechanics* 834:125–148, https://doi.org/10.1017/ jfm.2017.646.
- Voet, G., J.B. Girton, M.H. Alford, G.S. Carter, J.M. Klymak, and J.B. Mickett. 2015. Pathways, volume transport and mixing of abyssal water in the Samoan Passage. *Journal of Physical Oceanography* 45:562–588, https://doi.org/10.1175/ JPO-D-14-0096.1.
- Voet, G., M.H. Alford, J.B. Girton, G.S. Carter, J.B. Mickett, and J.M. Klymak. 2016. Warming and weakening of the abyssal flow through Samoan Passage. *Journal of Physical Oceanography* 46:2,389–2,401, https://doi.org/ 10.1175/JPO-D-16-0063.1.
- Whitehead, J.A., A. Leetmaa, and R.A. Knox. 1974. Rotating hydraulics of strait and sill flows. *Geophysical Fluid Dynamics* 6:101–125, https://doi.org/10.1080/03091927409365790.
- Whitehead, J.A. 1998. Topographic control of oceanic flows in deep passages and straits. *Reviews* of *Geophysics* 36:423–440, https://doi.org/ 10.1029/98RG01014.
- Whitehead, J.A. 2003. Constant potential vorticity hydraulically controlled flow: Complexities from passage shape. *Journal of Physical Oceanography* 33:305–312, https://doi.org/10.1175/1520-0485(2003)033<0305:CPVHCF>2.0.CO;2.

ACKNOWLEDGMENTS

We are grateful to Eric Boget, Andrew Cookson, Sam Fletcher, Trina Litchendorf, and Keith Magness for their assistance in the field program, and to the captains and crews of R/Vs Roger Revelle and Thomas G. Thompson for their excellent ship handling and assistance—without which this work would not have been possible. This work was supported by the National Science Foundation.

AUTHORS

James B. Girton (girton@uw.edu) is Principal Oceanographer, John B. Mickett is Senior Oceanographer, and ZhongXiang Zhao is Principal Oceanographer, all at the Applied Physics Laboratory, University of Washington, Seattle, WA, USA. Matthew H. Alford is Professor, Gunnar Voet is Assistant Project Scientist, and Jesse M. Cusack is Postdoctoral Researcher, all at Scripps Institution of Oceanography, University of California San Diego, La Jolla, CA, USA. Glenn S. Carter is Associate Professor, and Kelly A. Pearson-Potts is recent PhD, both in the Department of Oceanography, University of Hawai'i at Manoa, Honolulu, HI, USA. Larry J. Pratt is Senior Scientist, and Shuwen Tan is PhD Candidate, both at Woods Hole Oceanographic Institution, Woods Hole, MA, USA. Jody M. Klymak is Professor, University of Victoria, Victoria, British Columbia, Canada.

ARTICLE CITATION

Girton, J.B., J.B. Mickett, Z. Zhao, M.H. Alford, G. Voet, J.M. Cusack, G.S. Carter, K.A. Pearson-Potts, L.J. Pratt, S. Tan, and J.M. Klymak. 2019. Flowtopography interactions in the Samoan Passage. Oceanography 32(4):184–193, https://doi.org/10.5670/ oceanog.2019.424.

COPYRIGHT & USAGE

This is an open access article made available under the terms of the Creative Commons Attribution 4.0 International License (https://creativecommons.org/licenses/by/4.0/), which permits use, sharing, adaptation, distribution, and reproduction in any medium or format as long as users cite the materials appropriately, provide a link to the Creative Commons license, and indicate the changes that were made to the original content.